Separation Science and Technology
Publication details, including instructions for authors and subscription information:
http://www.informaworld.com/smpp/title~content=t713708471

Removal of Refractory Organics by Aeration. V. Solvent Sublation of Naphthalene and Phenanthrene

Shang-Da Huang[ab]; Kalliat T. Valsaraj[a]; David J. Wilson[a]
[a] DEPARTMENTS OF CHEMISTRY AND OF CIVIL AND ENVIRONMENTAL ENGINEERING, VANDERBILT UNIVERSITY, NASHVILLE, TENNESSEE [b] Department of Chemistry, National Tsing Hua University, Hsinchu, Taiwan, Republic of China

To cite this Article Huang, Shang-Da , Valsaraj, Kalliat T. and Wilson, David J.(1983) 'Removal of Refractory Organics by Aeration. V. Solvent Sublation of Naphthalene and Phenanthrene', Separation Science and Technology, 18: 10, 941 — 968
To link to this Article: DOI: 10.1080/01496398308060318
URL: http://dx.doi.org/10.1080/01496398308060318

SEPARATION SCIENCE AND TECHNOLOGY, 18(10), pp. 941-968, 1983

Removal of Refractory Organics by Aeration. V. Solvent Sublation of Naphthalene and Phenanthrene

SHANG-DA HUANG,* KALLIAT T. VALSARAJ, and DAVID J. WILSON†

DEPARTMENTS OF CHEMISTRY AND OF CIVIL AND ENVIRONMENTAL ENGINEERING
VANDERBILT UNIVERSITY
NASHVILLE, TENNESSEE 37235

Abstract

Naphthalene and phenanthrene are readily removed from aqueous systems by solvent sublation into mineral oil. The process is slightly enhanced by added salts, and slightly retarded by acetone and ethanol. The naphthalene results are used to test a mathematical model for solvent sublation column operation; satisfactory agreement is obtained.

INTRODUCTION

Solvent sublation, a surface chemical separation method originated by Sebba (*1*), has shown promise for the removal of some classes of organic compounds from wastewaters. Lemlich's book on adsorptive bubble separations includes a review on solvent sublation by Karger (*2*), and the subject is also covered in our recent book (*3*). Shorter reviews are included in our earlier papers (*4–7*). In solvent sublation a surface-active solute is transported from an aqueous phase to an overlying immiscible layer of a nonvolatile liquid on the air–water interfaces of bubbles rising through the solvent sublation column. Volatile solutes of low solubility in water may be removed in the interior of the bubbles in similar fashion by air stripping into

*Permanent address: Department of Chemistry, National Tsing Hua University, Hsinchu, Taiwan 300, Republic of China.

†To whom correspondence should be addressed.

 0149-6395/84/1810-0941$3.50/0

the organic layer. Lionel studied the sublation of volatile 1,1,1-trichloroethane and modeled the sublation of volatiles (*4*); Womack et al. analyzed the solvent sublation of neutral molecules, ion pairs, and ion triples from a single-stage, well-mixed system (*5*). We have modeled the sublation of surface-active substances from multistage columns in which axial dispersion is not sufficient to make the assumption of a single well-stirred pool a suitable approximation (*6*). Valsaraj has investigated the solvent sublation of dichlorobenzenes, a commercial polychlorinated biphenyl mixture, lindane, endrin, and two nitrophenols (*7*).

In a number of industrial processes wastes containing (possibly carcinogenic) polynuclear aromatic hydrocarbons are generated. We were interested in assessing the feasibility of using solvent sublation for removing these compounds from dilute aqueous systems, particularly in anticipation of synfuels development in this country in the future. We present here some experimental results on the solvent sublation of naphthalene and phenanthrene from water, including the effects of added salts and organic solvents. This is followed by the development of mathematical models describing the removal by solvent sublation of a solute which is both volatile and surface-active (as is the case with napthalene, for example). A method for estimating Langmuir parameters for hydrophobic solutes is then extended to these polynuclear aromatics, and the mass transfer rate coefficient is estimated. Finally, a comparison is made between the experimental and the calculated results.

EXPERIMENTAL

Apparatus

The apparatus consisted of a 3.5-cm diam × 85-cm high Pyrex column fitted with a stopper at the bottom through which passed a "fine" fritted glass gas dispersion tube and a sampling stopcock. House air was passed through a water saturator and glass wool filter before going to the gas dispersion tube. Air flow rates were adjusted with a needle valve and measured with a soap film flowmeter. Air flow rates were kept at 97 mL/min for all runs.

Fisher laboratory grade naphthalene or Eastman phenanthrene were "dissolved" in distilled water by stirring with a magnetic stirrer for 24 h. The solutions were filtered through a sintered glass filter to remove suspended solids. The concentrations of the sample solutions so prepared were 21 to 30 mg/L naphthalene or 1.3 to 1.4 mg/L phenanthrene. The solubilities of naphthalene and phenanthrene listed in the literature (*8, 9*) were 30 and 2.7 mg/L, respectively.

The volume of the sample solution used was 200 mL for the runs made with naphthalene and 250 mL for the runs made with phenanthrene. The solution was poured into the column, and 5 mL of paraffin oil (Fisher Laboratory grade) was added immediately and the timer started. Five milliliters of naphthalene solution or 200 mL of phenanthrene solution was taken for analysis. The standard solutions were prepared by dissolving naphthalene or phenanthrene in hexane (Fisher pesticide grade). The concentrations of the samples were measured with a Shimadzu GC-MINI 2 Gas Chromatograph with a C-R1B Chromatopac integrater and a flame ionization detector. A 52-m Chrompack glass capillary column, coated with SE-30, was used. The capillary column temperature was set at 200°C.

Data were plotted as percentage of sample remaining in solution versus time in minutes on a semilog scale to clearly display any deviation from first-order kinetics, which would yield linear plots.

All runs were made at room temperature.

RESULTS

The rates of separation of naphthalene from aqueous solutions by solvent sublation and by aeration (without an organic layer on the top of the separation column) are shown in Fig. 1. The runs followed first-order kinetics approximately; 98% of the naphthalene was removed by solvent sublation in 2 h. The residual naphthalene concentration was less than 1 ppm. Only 88% of the naphthalene was removed by simple aeration for 2 h. The first-order rate constants for the separations are listed in Table 1. The rate constant for solvent sublation is more than twice as large as that for simple aeration. The improvement in separation is presumably due to the surface adsorption of surface-active napthalene on the surface of the bubbles; the surface-adsorbed naphthalene and the naphthalene in the vapor phase inside the bubble are carried into the organic layer on the top of the separation column during solvent sublation. Only the naphthalene vapor inside the air bubble is removed by simple aeration. Naphthalene is fairly volatile; its vapor pressure at room temperature is 0.165 mmHg (*10*).

The effects of added salts on the solvent sublation of naphthalene are shown in Fig. 2 and in Table 1. We see that the presence of salts increases the rate of the separation somewhat. Presumably this is due to the same mechanism that causes the widely used "salting out" effect in which organics are made less soluble in aqueous phases by the addition of salts. These tie up water molecules in ion hydration shells, thereby decreasing the amount of water available for solubilizing the organic.

The influence of organic solvents, such as ethanol, is exhibited in Fig. 3 and Table 1. The rate of separation decreased somewhat with increasing ethanol concentration. This is probably due to attractive forces between naphthalene and ethanol molecules, which would increase the solubility of

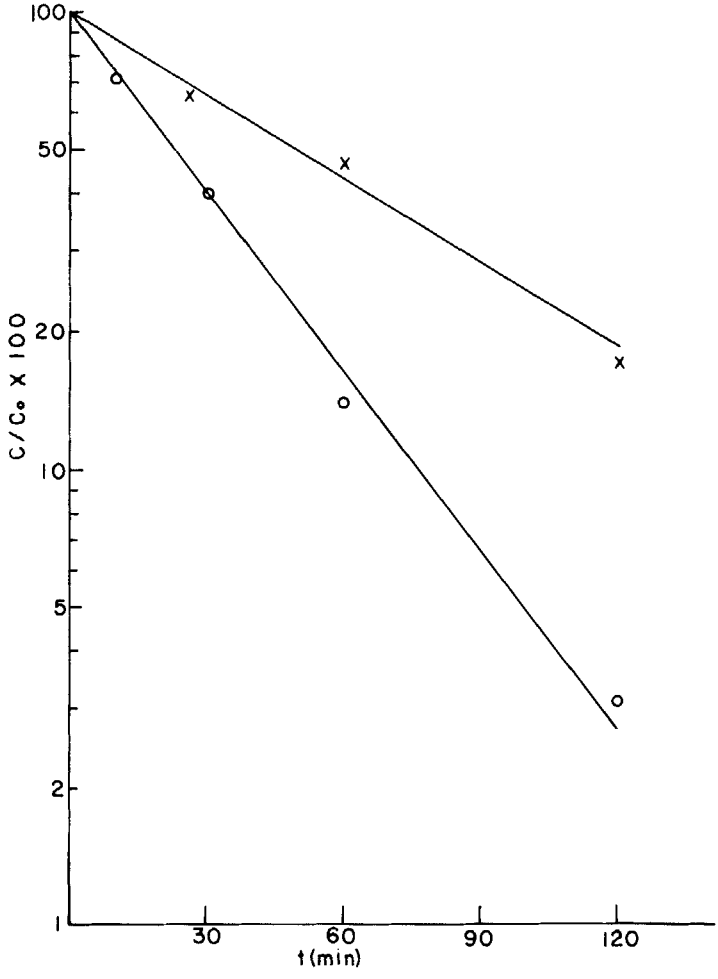

FIG. 1. Removal of naphthalene from aqueous solution by solvent sublation (○) and by aeration alone (×).

TABLE 1
Separation Rate Constants for Solvent Sublation and Aeration of Naphthalene Aqueous Solutions

Composition of aqueous phase	Rate constant $K \times 10^4$ (s^{-1})
H_2O	5.00
H_2O	2.38
2% $NaNO_3$	5.58
2% $AgNO_3$	5.58
20% $NaNO_3$	9.31
2% Ethanol	4.40
5% Ethanol	4.16
10% Ethanol	3.51
2% Acetone	4.87

naphthalene in the solution. The value of the separation rate constant for a solution containing 10% by volume ethanol is 71% of its value for naphthalene removal from water alone. We found 92% removal of naphthalene in 2 h from the solution containing 10% ethanol.

Acetone produces a smaller effect on the rate of separation than does ethanol, as seen in Fig. 4 and Table 1. The value of the separation rate constant for the solution containing 2% acetone is 97% of its value for naphthalene removal in the absence of acetone. The corresponding figure for the removal of naphthalene from water–2% ethanol is 88%. The difference between ethanol and acetone may be due in part to increased volatilization of low-boiling acetone.

The removal of phenanthrene by solvent sublation is shown in Fig. 5 and Table 2. The rate constant for the separation by solvent sublation is three times as large as that for removal by aeration alone.

MODELS OF SOLVENT SUBLATION

Here we first examine mathematical models for the operation of a single-stage (well-stirred pool) solvent sublation apparatus; we assume that the process is equilibrium controlled. Batch and steady-state continuous flow modes are analyzed. Then we develop a substantially more complex model for the operation of a multistage column in which the process is limited by the rate of diffusion of solute through the boundary layers of liquid around the rising bubbles.

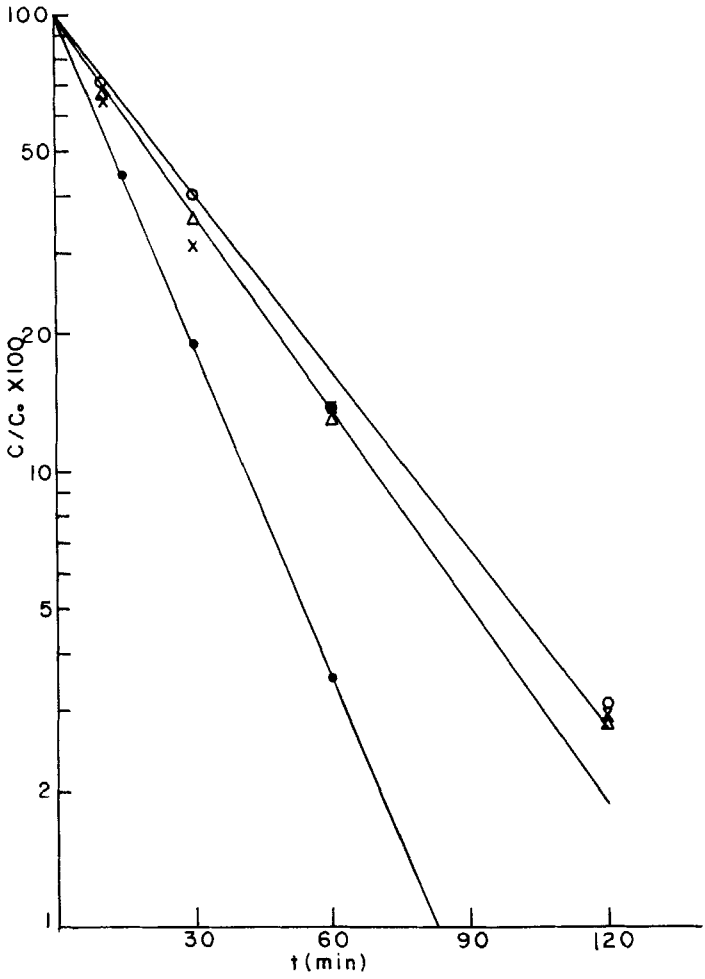

FIG. 2. Effect of salts on solvent sublation of naphthalene: (○) water, (△) 2% $AgNO_3$, (×) 2% $NaNO_3$, (●) 20% $NaNO_3$.

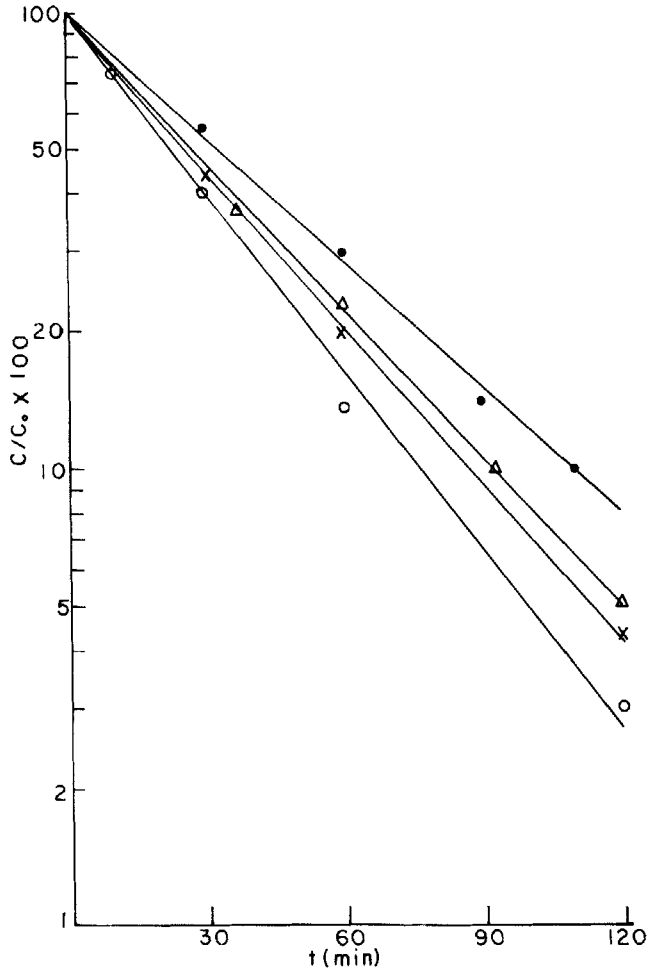

FIG. 3. Effect of ethyl alcohol on solvent sublation of naphthalene: (○) water, (×) 2% alcohol, (△) 5% alcohol, (●) 10% alcohol.

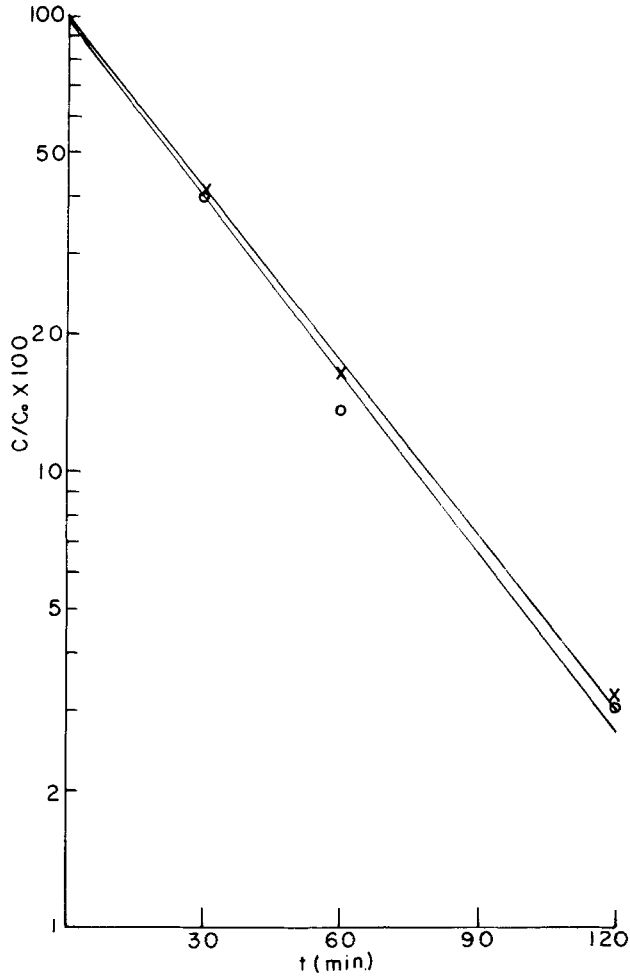

FIG. 4. Effect of acetone on solvent sublation of naphthalene: (○) water, (×) 2% acetone.

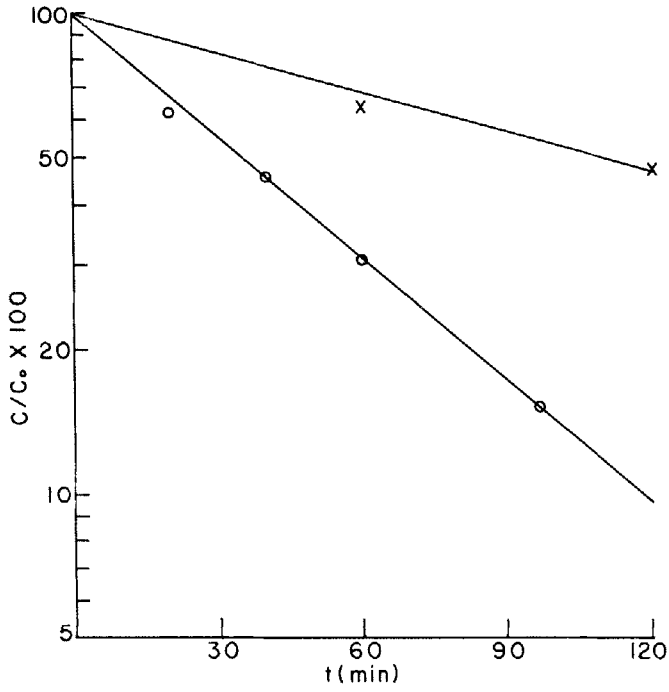

FIG. 5. Removal of phenanthrene from aqueous solution by solvent sublation (○) and by aeration alone (×).

TABLE 2
Separation Rate Constants for Solvent Sublation and Aeration of Phenanthrene Aqueous Solution

Composition of aqueous phase	Rate constant $K \times 10^4$ (s^{-1})
H_2O	3.24
H_2O	1.08

Single-Stage, Equilibrium-Controlled Operation

We assume that the concentration of solute in the vapor within a bubble is given by Henry's law,

$$c_g = Kc_w \tag{1}$$

where c_g = vapor-phase solute concentration, g/cm^3
K = Henry's law constant
c_w = aqueous phase solute concentration, g/cm^3

The surface concentration of solute we take as

$$\Gamma = \Gamma_m c_w/(c_{1/2} + c_w) \tag{2}$$

where Γ_m = Langmuir parameter, g/cm^2
$c_{1/2}$ = Langmuir parameter, g/cm^3
Γ = surface concentration, g/cm^2

The mass of solute carried out of the solution by one bubble is then given by

$$m = VKc_w + S\Gamma_m c_w/(c_w + c_{1/2}) \tag{3}$$

where $V = (4/3)\pi r_b^3$
$S = 4\pi r_b^2$
r_b = bubble radius

For an apparatus operating in the batch mode, the rate of change of c_w with time is given by

$$dc_w/dt = -Nm/V_w \tag{4}$$

where N = number of bubbles formed per sec
$= Q_a/V$ (5)
Q_a = airflow rate
V_w = volume of the column's aqueous phase

On substituting Eqs. (3) and (5) into (4), we obtain

$$\frac{dc_w}{dt} = \frac{-Q_a}{VV_w}\left[VKc_w + \frac{S\Gamma_m c_w}{c_w + c_{1/2}}\right] \tag{6}$$

Rearrangement of this equation yields

$$\frac{c_w + c_{1/2}}{c_w} \frac{dc_w}{VKc_w + (VKc_{1/2} + S\Gamma_m)} = \frac{-Q_a}{VV_w} \, dt \tag{7}$$

This can be integrated by partial fractions to give

$$(1 + A)^{-1} \log \frac{c_w}{c_w^0} + A(1 + A)^{-1} \log \frac{c_w + B}{c_w^0 + B} = \frac{-KQ_a t}{V_w} \tag{8}$$

where $A = 3\Gamma_m/(rKc_{1/2})$ (9)

$B = c_{1/2} + (3\Gamma_m/rK)$
$c_w^0 =$ initial solute concentration (10)

From Eq. (8) we can readily determine the time required to remove, say, 99% of the initial solute.

We turn next to a single-stage continuous-flow apparatus operating in a steady-state. For this we have

$$Q_w c_{\text{infl}} = Q_w c_w + Q_a K c_w + \frac{Q_a S_b}{V_b} \frac{\Gamma_m c_w}{c_w + c_{1/2}} \tag{11}$$

as the mass balance. This equation rearranges to give a quadratic equation in c_w,

$$0 = (Q_w + Q_a K)c_w^2 + (Q_w c_{1/2} + Q_a K c_{1/2} + 3Q_a \Gamma_m / r_b - Q_w c_{\text{infl}})c_w - Q_w c_{\text{infl}} c_{1/2} \tag{12}$$

We introduce a more abbreviated notation,

$$\alpha = Q_w + Q_a K \tag{13}$$

$$\beta = (Q_w c_{1/2} + Q_a K c_{1/2} + 3Q_a \Gamma_m / r_b - Q_w c_{\text{infl}}) \tag{14}$$

$$\gamma = Q_w c_{\text{infl}} c_{1/2} \tag{15}$$

Then

$$c_w = [-\beta + (\beta^2 + 4\alpha\gamma)^{1/2}]/2\alpha \tag{16}$$

gives us the steady-state effluent concentration.

Multistage, Kinetically Controlled Operation

The above treatment assumes that diffusion of solute to the bubbles through their boundary layers is sufficiently rapid that it maintains the bubble in equilibrium with the bulk solution surrounding it. That treatment also approximates the aqueous phase in the column as a well-stirred pool. In this section we relax both these constraints.

We partition the aqueous phase in our solvent sublation column into N equal-sized slabs, and do the usual material balance on each slab to obtain

$$\frac{dc_i}{dt}\pi R^2 \Delta h = Q_w(c_{i+1} - c_i) + J(m_{i-1} - m_i) + \frac{\pi R^2 D_{ax}}{\Delta h}(c_{i+1} - 2c_i + c_{i-1}) \qquad (17)$$

$$\frac{dc_1}{dt}\pi R^2 \Delta h = Q_w(c_2 - c_1) - Jm_1 + \frac{\pi R^2 D_{ax}}{\Delta h}(c_2 - c_1)$$

$$\frac{dc_N}{dt}\pi R^2 \Delta h = Q_w(c_{infl} - c_N) + J(m_{N-1} - m_N) + \frac{\pi R^2 D_{ax}}{\Delta h}(c_{N-1} - c_N)$$

where R = column radius
$\Delta h = h/N$
h = height of aqueous column
J = number of bubbles discharged per second
c_i = solute concentration in the ith slab
m_i = mass of solute associated with a bubble at the top of the ith slab
D_{ax} = axial dispersion constant
Q_w = influent flow rate

We assume that the m_i are determined by

$$\frac{dm_i}{dt} = 4\pi r_i^2 k(c_i - c_i') \tag{18}$$

where k = mass transfer rate coefficient, cm/s
r_i = bubble radius in ith slab

Here c_i is the concentration of solute in the inner side of the bubble boundary layer, immediately adjacent to the air–water interface. The relationship between c_i' and m_i is given by

$$m_i = 4\pi r^2 \Gamma_m c_i'/(c_i + c_{1/2}) + \tfrac{4}{3} r_i^3 K c_i' \tag{19}$$

Here Γ_m = Langmuir parameter, g/cm^2
$c_{1/2}$ = Langmuir parameter, g/cm^3
K = Henry's law constant, dimensionless

The first term in this equation gives us the mass of solute on the surface of the bubble; the second, the mass of solute in the vapor phase. Equation (18) assumes that Fick's first law is applicable to calculating diffusional mass transfer through the bubble boundary layers. We let

$$S_i = 4\pi r_i^2 \tag{20}$$

$$V_i = \tfrac{4}{3}\pi r_i^3 \tag{21}$$

We next make the approximation that the change in the c_i during the time interval required for a bubble to traverse one slab is negligible, so that c_i may be treated as a constant in Eq. (18). It is then possible, by use of Eq. (19), to integrate Eq. (18) over the time interval required for a bubble to rise through a slab, thereby determining the increase in solute mass associated with the bubble as it transits the slab. This can be done by noting that

$$\frac{dm_i}{dt} = \frac{dm_i}{dc_i}\frac{dc_i'}{dt} \tag{22}$$

and that

$$\frac{dm_i}{dc_i'} = \frac{S_i \Gamma_m c_{1/2}}{(c_{1/2} + c_i')^2} + V_i K \tag{23}$$

These relationships allow us to transform Eq. (18) into

$$\frac{dc_i'}{dt} = S_i k(c_i - c_i')/\left[\frac{S_i\Gamma_m c_{1/2}}{(c_{1/2} + c_i')^2} + V_i K\right] \tag{24}$$

This is readily integrated by separating the variables and use of partial fractions; the final result is

$$\frac{S_i\Gamma_m c_{1/2}}{(c_i + c_{1/2})^2} \log\left\{\frac{[c_i'(t) + c_{1/2}][c_i - c_i'(0)]}{[c_i'(0) + c_{1/2}][c_i - c_i'(t)]}\right\} + V_i K \log\frac{c_i - c_i'(0)}{c_i - c_i'(t)}$$

$$+\frac{S_i\Gamma_m c_{1/2}}{c_i + c_{1/2}}\left[\frac{1}{c_i'(0) + c_{1/2}} - \frac{1}{c_i'(t) + c_{1/2}}\right] = S_i kt \tag{25}$$

This can be solved numerically for $c_i'(t)$; the value of $c_i'(0)$ to be used is the value obtained from Eq. (19) by replacing m_i by $m_{i-1}(\Delta h/u_{i-1})$, $i > 1$, or by 0, $i = 1$, and solving for c_i'. Here u_j is the bubble rise velocity in the jth slab, calculated iteratively from

$$u_j \equiv u = \frac{2g\rho r_j^2}{9\eta\left[1 + 1/4\left(\frac{\rho r_j u}{2\eta}\right)^{1/2} + 0.34\frac{\rho r_i u}{12\eta}\right]} \tag{26}$$

where g = gravitational constant
ρ = liquid density
r_j = bubble radius in the jth slab
η = viscosity, poise

The numerical solution of Eq. (25) is rather time consuming, since it involves the calculation of many logarithms; this must be done very many times during the computer simulation of a run. We therefore seek an alternative approach.

We rewrite Eq. (19) as a quadratic in c_i', obtaining

$$V_i K(c_i')^2 + (S_i\Gamma_m + V_i K c_{1/2} - m_i)c_i' - m_i c_{1/2} = 0 \tag{27}$$

or

$$A_i(c_I')^2 + B_i c_i' + C_i = 0$$

Then

$$c_i' = [-B_i + (B_i^2 - 4A_iC_i)^{1/2}]/2A_i \tag{28}$$

One sees that the positive sign in the quadratic formula is needed in order that

$$\lim c_i' \to 0$$
$$m_i \to 0 \tag{29}$$

The bubble volumes in the various slabs, V_i, are related to the bubble volume at one atmosphere, V, by

$$V_i = \frac{V \times 1.013 \times 10^6}{1.013 \times 10^6 + (N - i + 1/2)\rho g \Delta h + \rho_0 g h_0} \tag{30}$$

where 1.013×10^6 = atmospheric pressure in dyn/cm^2
ρ_0 = density of the organic solvent on top of the water column, g/cm^3
h_0 = thickness of the organic solvent layer

Then the bubble radii and surface areas are given by

$$r_i = r(V_i/V)^{1/3} \tag{31}$$

$$S_i = S(V_i/V)^{2/3} \tag{32}$$

where r and S are the radius and the surface area of a bubble at atmospheric pressure, respectively.

Now the time scale required for the integration of Eq. (18) is relatively short, and is determined by the bubble boundary layer thickness and the solute diffusion constant. This dictates small values of δt. The duration of a column run, however, may be an hour or more, so we see that computer costs may be quite large. We can reduce the amount of computer time required very substantially by the following procedure. We use two time increments, a small one (δt) and a large one (Δt). We select δt to be suitable for the integration of Eq. (18) over the time intervals $\tau_i = u_i/\Delta h$ required for a bubble to rise through one slab. We select Δt to be suitable for integrating Eq. (17); during the time interval Δt the fractional changes in the c_i should be small. Typically, δt might be roughly $\tau_i/20$ while Δt might be of the order of $10\tau_i$. Thus, the time intervals over which we must use the short time increment δt in integrating Eq. (18) are $(0, \tau_i)$, $(\Delta t, \Delta t + \tau_i), \ldots,$ $(n\Delta t, n\Delta t + \tau_i), \ldots$. We see that this eliminates about nine-tenths of the numerical integration of Eq. (18) which would be needed if we used the same time interval for integrating both Eqs. (17) and (18). This results in an increase in program speed by a factor of the order of five.

Mass Transfer Rate Coefficients

The diffusion equation in the case of spherical coordinates is

$$\frac{\partial c}{\partial t} = \frac{D}{r^2}\frac{\partial}{\partial r}\left(r^2\frac{\partial c}{\partial r}\right), \qquad a \le r \le b \tag{33}$$

where D = diffusion constant
a = bubble radius
b = radius of bubble plus boundary layer

This equation is readily solved by separation of variables to yield

$$c(r, t) = \frac{A_0}{r} + B_0 + \frac{1}{r}\sum\left[A_\lambda \sin\sqrt{\frac{\lambda}{D}}\, r + B_\lambda \cos\sqrt{\frac{\lambda}{D}}\, r\right] \exp(-\lambda t) \tag{34}$$

Mass balance considerations give

$$\frac{dm_b}{dt} = 4\pi a^2 D\frac{\partial c}{\partial r}, \; r = a \tag{35}$$

where m_b = mass of solute in, and on the surface of, the bubble

Recall

$$m_b = \frac{4\pi a^2 \Gamma_m c(a, t)}{c(a, t) + c_{1/2}} + \tfrac{4}{3}\pi a^3 K c(a, t) \tag{19'}$$

so

$$\frac{dm_b}{dt} = \tfrac{4}{3}\pi a^3 K\frac{\partial c(a, t)}{\partial t} + \frac{4\pi a^2 \Gamma_m c_{1/2}}{[c(a, t) + c_{1/2}]^2}\frac{\partial c(a, t)}{\partial t} \tag{36}$$

To make further progress we must assume that $c_{1/2} \gg c(a, t)$, which linearizes Eq. (36),

$$\frac{dm_b}{dt} = \left[\tfrac{4}{3}\pi a^3 K + \frac{4\pi a^2 \Gamma_m}{c_{1/2}}\right]\frac{\partial c(a, t)}{\partial t} \tag{37}$$

Equating Eq. (35) to Eq. (37) then yields

$$\frac{\partial c(a,\ t)}{\partial t} = \frac{D}{\alpha}\frac{\partial c(a,\ t)}{\partial r} \tag{38}$$

where

$$\alpha = \frac{aK}{3} + \frac{\Gamma_m}{c_{1/2}}$$

Equation (38) serves as one of our boundary conditions. The boundary condition at $r = b$ is simply

$$c(b,\ t) = c_\infty \tag{39}$$

where c_∞ is the bulk concentration.

From here on the analysis is straightforward. Substitution of Eq. (34) into Eqs. (38) and (39) gives a pair of linear homogeneous equations for A_λ and B_λ; nonzero values for these dictate that the determinant of the coefficients of this system be zero. This yields the following eigenvalue equation.

$$\tan\left[\left(\frac{\lambda}{D}\right)^{1/2}(b-a)\right] = \frac{\dfrac{1}{\alpha}\left(\dfrac{\lambda}{D}\right)}{\dfrac{\lambda}{D}\dfrac{1}{\alpha a}} \tag{40}$$

We next relate the smallest positive eigenvalue of Eq. (40) to the mass transfer rate coefficient k. From Eq. (18) we have

$$\frac{dm_b}{dt} = 4\pi a^2 k[c_\infty - c(a,\ t)] \tag{41}$$

We also have

$$\frac{dm_b}{dt} = \left[\frac{4\pi a^3 K}{3} + \frac{4\pi a^2 \Gamma_m}{c_{1/2}}\right]\frac{\partial c(a,\ t)}{\partial t} \tag{37'}$$

On keeping only the first eigenvalue λ_1 in Eq. (34) and using the initial condition $c(a,\ 0) = 0$, we find

$$c(a,\ t) = c_\infty[1 - \exp(-\lambda_1 t)] \tag{42}$$

Differentiating yields

$$\frac{\partial c(a, t)}{\partial t} = \lambda_1 c_\infty - \lambda_1 c(a, t) \tag{43}$$

Substituting Eq. (43) into Eq. (37′) yields

$$\frac{dm_b}{dt} = \left[\frac{4\pi a^3 K}{3} + \frac{4\pi a^2 \Gamma_m}{c_{1/2}}\right] \lambda_1 [c_\infty - c(a, t)] \tag{44}$$

Comparison of this with Eq. (41) gives

$$4\pi a^2 k = \left[\frac{4\pi a^3 K}{3} + \frac{4\pi a^2 \Gamma_m}{c_{1/2}}\right] \lambda_1$$

or

$$k = \lambda_1 \left[\frac{aK}{3} + \frac{\Gamma_m}{c_{1/2}}\right] \tag{45}$$

as the relationship between our least positive eigenvalue and the mass transfer rate coefficient. Equation (40) is readily solved graphically or numerically for λ_1.

THEORETICAL RESULTS

In this section we discuss first the dependence of the behavior of a solvent sublation column upon various parameters appearing in our mathematical model of column operation. We then explore the possibility of duplicating the experimental results presented earlier in this paper for naphthalene and phenanthrene. The algorithm used for integrating the differential equations forward in time was Heun's predictor-corrector method (*11*). The standard set of parameters used in testing the program is listed in Table 3. We note that the Henry's law constant is given by

$$K = \frac{P_{\text{vap}} \times (\text{mol. wt.})/760 \times 82.05 \times T}{\text{aqueous solubility of solute, g/mL}} \tag{46}$$

where P_{vap} is in mmHg

TABLE 3
Standard Input Parameters for Program Simulating Solvent Sublation of a Volatile Surface-Active Solute

Parameter	Value
Number of slabs into which the column is partitioned	2
Δt	40 s
Number of cycles between printouts	25
Air flow rate	5.0 mL/s
Flow rate of influent	0.0 mL/s
Height of an aqueous slab	50.0 cm
Radius of the column	1.6 cm
Initial radius of the bubble	0.02 cm
Influent concentration	2.03×10^{-7} mol/mL
Axial dispersion coefficient	0.0
$c_{1/2}$	1.08×10^{-5} mol/mL
Γ max	4.2×10^{-10} mol/cm^2
Solubility in water at 25°C	3.0×10^{-5} g/mL
Vapor pressure at 25°C	0.1652 mmHg
Density of aqueous solution	0.9952 g/mL
Density of organic solvent	0.8450 g/mL
Viscosity of water	0.01002 P
Viscosity of organic solvent	0.2366 P
Height of the organic layer	2.0 cm
Mass transfer coefficient	4.83×10^{-6} cm/s
Molecular weight of the solute	128.16 g/mol

The solute parameters were selected to correspond to naphthalene, and the column parameters corresponded to our lab scale batch apparatus.

The effect of varying the bubble radius (at 1 atm) is shown in Fig. 6. We see that decreasing the bubble size results in a very marked increase in the rate of removal. This is due both to the increased surface area of the bubbles (per unit volume of air) and to the increased contact time of the bubbles with the liquid as the bubble radius is decreased. Exponential curves give quite good fits to the calculated results, as indicated in Table 4.

The effects of varying the mass transfer rate coefficient are shown in Fig. 7. The expected increase in removal rate with increasing k is seen. It is evident that even the largest values of k used are not large enough to result in the process being equilibrium-controlled, under which circumstances the plots would approach a limiting curve. Table 5 gives the removal rate constants for exponential fits to the calculated curves.

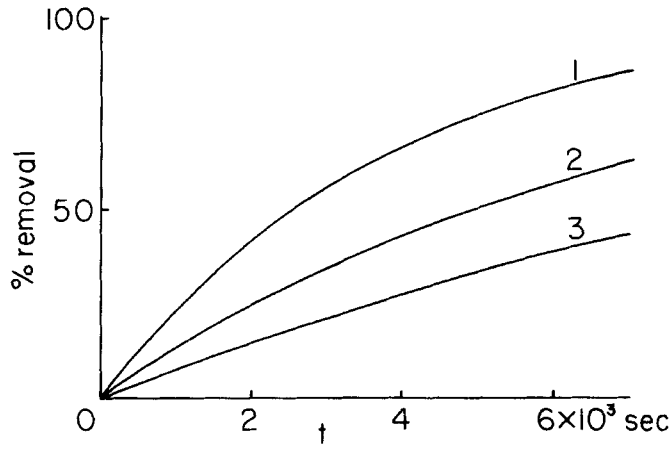

FIG. 6. Effect of bubble radius r_b on solvent sublation. $r_b = 0.010$, 0.015, 0.020 cm (top to bottom); other parameters as in Table 3.

As one would expect, the rate of removal was directly proportional to the air flow rate. We see in Fig. 8 the effect of increasing the Langmuir parameter $c_{1/2}$, which corresponds to weakening the binding of the adsorbed molecules. This produces a decrease in removal rate. The effects of increasing Γ_m are shown in Fig. 9; increasing Γ_m increases the maximum number of solute molecules which can be adsorbed at the interface, and so increases the rate of removal of solute, as seen.

We chose three different vapor pressures (0.001652, 0.1652, and 1.652 mmHg) from which to calculate the Henry's law constant; the effects of

TABLE 4
Effect of Bubble Radius on Removal Rates

r (cm)	Removal rate constant k' (s^{-1})	Standard deviation σ_k (s^{-1})
0.01	2.802×10^{-4}	3.128×10^{-8}
0.015	1.423	2.128×10^{-9}
0.02	0.8228	7.100×10^{-10}

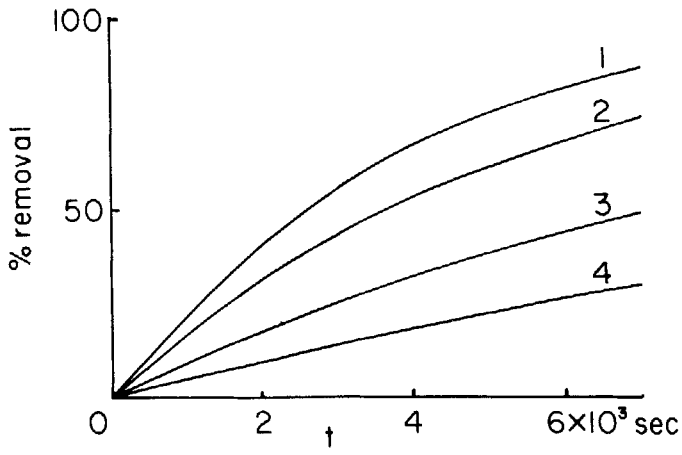

FIG. 7. Effect of mass transfer rate coefficient k on solvent sublation. $k = 4.83$, 2.50, 1.00, and 0.483×10^{-7} cm/s (top to bottom); other parameters as in Table 3.

varying K in this way are shown in Fig. 10. The removal shown in the bottom curve is associated almost completely with the surface activity of the solute.

The number of slabs into which the column is partitioned can be profitably used to take into account the extent of axial mixing in the column; the more slabs, the less axial mixing. This is a much more economical way of dealing with axial mixing than using a large number of slabs and adjusting the axial dispersion constant D_{ax}. In Fig. 11 we see (on a logarithmic scale) the results of increasing the number of slabs from 1 to 10. This results in a modest

TABLE 5
Effect of Mass Transfer Rate Coefficient on Removal Rates

k (cm/s)	k' (s^{-1})	σ_k (s^{-1})
0.483×10^{-6}	0.5075×10^{-4}	0.07195×10^{-8}
1.00	0.9577	0.04608
2.50	1.905	0.6562
4.83	2.802	3.128

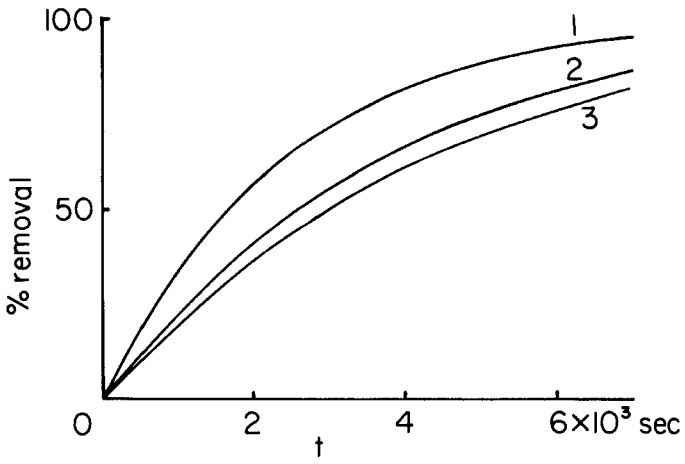

FIG. 8. Effect of Langmuir parameter $c_{1/2}$ on solvent sublation. $c_{1/2} = 0.108$, 1.08, 10.8×10^{-5} mol/cm^3 (top to bottom); other parameters as in Table 3.

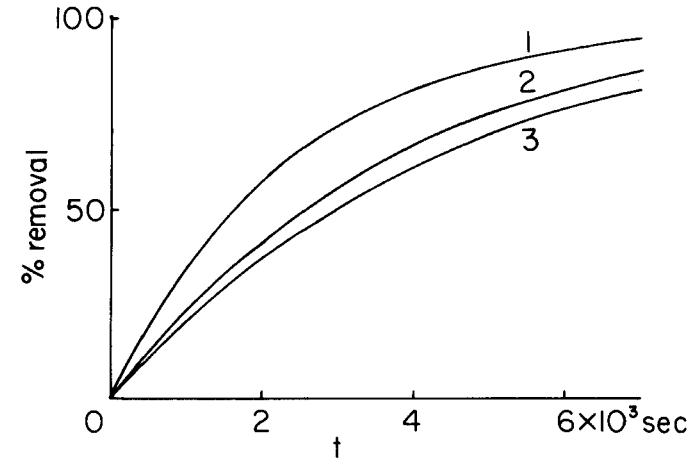

FIG. 9. Effect of Langmuir parameter Γ_m on solvent sublation. $\Gamma_m = 42$, 4.2, 0.42×10^{-10} mol/cm^2 (top to bottom); other parameters as in Table 3.

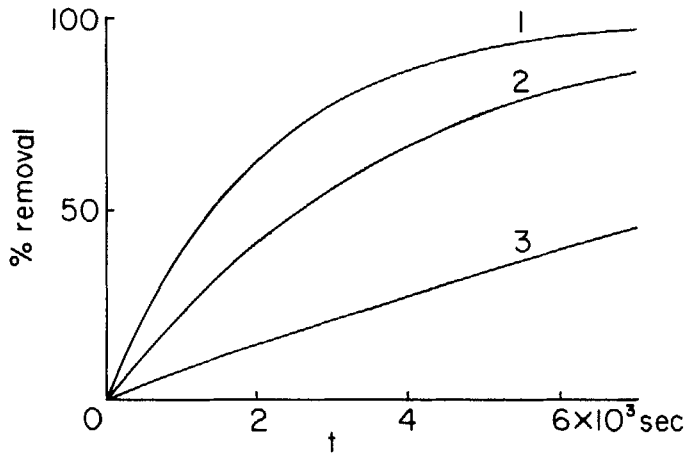

FIG. 10. Effect of Henry's law constant K on solvent sublation. $K = 38.61$, 3.861, 0.03861×10^{-2} (top to bottom); other parameters as in Table 3.

increase in removal rate in these batch runs, but it is evident that the dividends resulting from careful reduction of axial dispersion in batch solvent sublation columns will be relatively slight.

Comparison of Theory and Experiment

Here the mathematical model for solvent sublation described above is tested against the data reported in this paper on the solvent sublation of naphthalene into mineral oil. The column dimensions used were as listed in Table 3, and an air flow rate of 1.6 mL/s was used. The physical constants for naphthalene which are needed are given in Table 6.

In order to estimate the Langmuir parameter $c_{1/2}$ for naphthalene, we need the interfacial tension of the naphthalene–water system. This was calculated using the Girifalco-Good equation (*16*)

$$\gamma_{ab} = \gamma_a + \gamma_b - 2\phi(\gamma_a\gamma_b)^{1/2} \tag{47}$$

where γ_a and γ_b are the surface tensions of the pure species against air and ϕ is a constant which is approximately 0.7 for aromatic hydrocarbons. On using $\gamma(H_2O) = 72.75$ and $\gamma(\text{naphthalene}) = 40.07$, we obtain $\gamma(\text{naph-}$

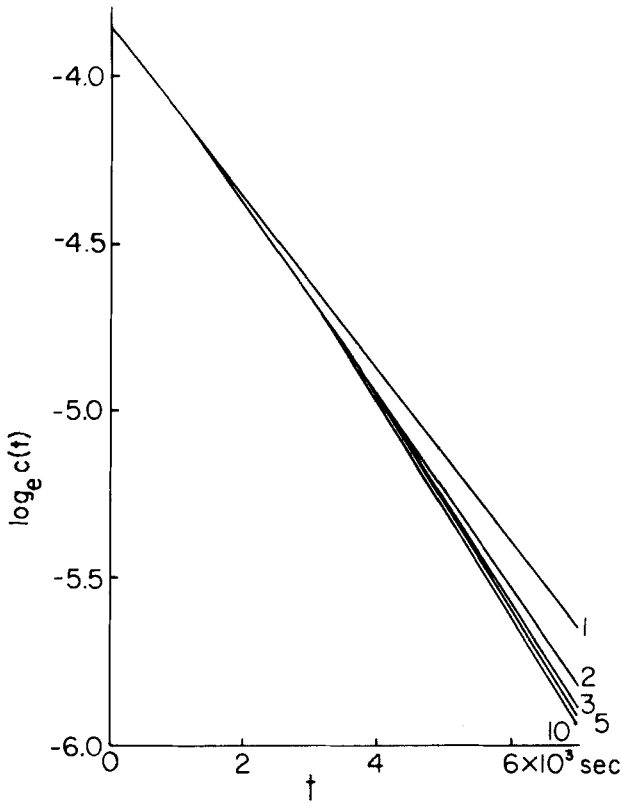

FIG. 11. Effect of number of slabs (axial dispersion) on solvent sublation. The number of slabs used to represent the column in each simulation is indicated in the figure; other parameters as in Table 3.

TABLE 6
Physical Constants for Naphthalene at 25°C

Parameter	Value
Molecular weight	128.16
Density (*12*)	1.145 g/mL
Solubility in water (*13*)	30 mg/L
Surface tension against air[a] (*14*)	40.07 dyn/cm
Vapor pressure[a] (*15*)	0.1652 mmHg

[a]The value at 25°C was obtained by extrapolating the data given.

TABLE 7
Derived Parameters for Naphthalene

Parameter	Value
γ(Naphthalene/H_2O)	37.2 ergs/cm^2
Molecular area	39 Å^2
Molecular volume	1.858×10^{-22} cm^3
Molecular adsorption energy, V_0	-2.76×10^{-13} erg/molecule
$c_{1/2}$	1.08×10^{-5} mol/cm^3
Γ_m	4.2×10^{-10} mol/cm^2
Diffusion constant D	6.16×10^{-6} cm^2/s
Henry's law constant, K	0.03861

thalene/H_2O) = 37.2 ergs/cm^2. We estimate from models that the area occupied by a naphthalene molecule lying flat on the air–water interface is 39 Å^2. Values of $c_{1/2}$ and Γ_m were then calculated by the prescription described in an earlier paper (*7*). Henry's law constant was calculated from Eq. (46). The derived parameters for naphthalene are given in Table 7.

We can use these values of $c_{1/2}$, Γ_m, and K to calculate the amount of naphthalene that would be carried in the vapor phase and on the surface of a bubble at equilibrium in a saturated solution of naphthalene in water. If the bubble has a radius of 0.0125 cm,

$$m(\text{vapor}) = \tfrac{4}{3}\pi r_b^3 Kc(\text{satd})(\text{mol. wt.})$$
$$= 9.32 \times 10^{-12} \text{ g}$$

$$m(\text{surface}) = \frac{4\pi r_b^2 \Gamma_m c}{c_{1/2} + c}(\text{mol. wt.})$$
$$= 2.24 \times 10^{-12} \text{ g}$$

We see that about 80% of the naphthalene is carried in the vapor phase. We warn that this estimate is only rough, since the value of $c_{1/2}$ selected has a marked effect on the extent of surface adsorption. The value of this parameter is rather uncertain, since it depends exponentially on V_0, the molecular adsorption energy, which in turn depends on the accuracy of Eq. (47) in estimating γ(naphthalene/H_2O) and on our estimate of the surface area occupied by a molecule. Nevertheless, the calculations indicate that naphthalene is both volatile and surface-active.

Other parameters needed are the bubble radius, the boundary layer thickness around the bubble, and the mass transfer rate coefficient. We

TABLE 8
Mass Transfer Rate Coefficients for Naphthalene

Bubble radius (cm)	k (cm/s)
0.010	4.15×10^{-5}
0.015	5.00
0.020	5.72

estimated the range of bubble radii photographically, observing a range of diameters from 0.02 to 0.1 cm, with a preponderance of small bubbles, especially in the lower portion of the column. We therefore decided to carry out our calculations using bubble radii between 0.01 and 0.02 cm. The boundary layer thicknesses for these bubbles were then calculated using the procedure described earlier (*7*). The boundary layer thicknesses were approximately 0.01 cm, and showed little variation for bubbles having radii in the range 0.01 to 0.02 cm (0.0101 to 0.0118 cm, respectively). The mass transfer rate coefficients were calculated for these bubbles by solving Eq. (40) graphically, with the results shown in Table 8.

These values of the mass transfer rate coefficient and the bubble radius were used in the mathematical model, which was then fitted to the experimental results by adjusting $c_{1/2}$, the parameter which we felt had the greatest uncertainty. The experimental column appeared to have a good deal of axial mixing, so we used only two slabs to represent the column (which gives a great deal of axial mixing), and then set $D_{ax} = 0$. Figure 12 shows a plot of an experimental run for naphthalene (circles) together with simulations for bubble radii of 0.01 and 0.015 cm. The values of $c_{1/2}$ and V_0 required to get these fits are given in Table 9, together with the percent discrepancy between the fitted value V_0(expt) and the value of V_0 calculated by the procedure outlined above, V_0(calc).

CONCLUSIONS

We conclude that the agreement between the theory and the experimental data is quite satisfactory, especially when one considers the uncertainty inherent in our estimation of the surface binding energy V_0. We note that the model predicts markedly increased rates of removal with decreased bubble size, due to (a) more surface area per unit volume of air, which facilitates removal through surface adsorption, and (b) longer contact times of the smaller, more slowly rising bubbles, which facilitates mass transport through the bubble boundary layer. The model developed earlier (*7*) for estimating Langmuir parameters appears to be a useful (though hardly a highly precise)

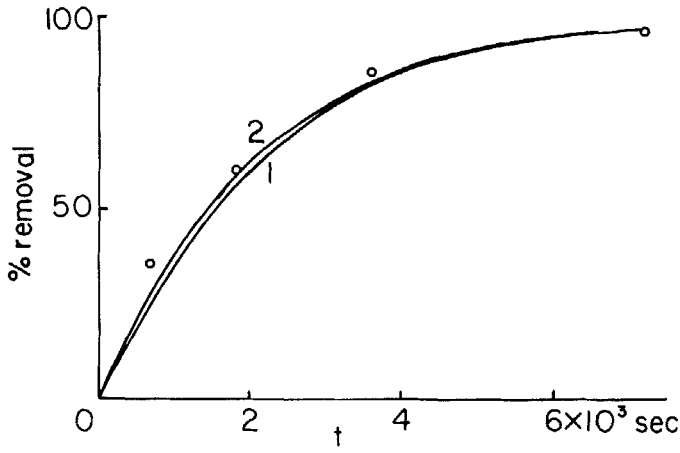

FIG. 12. Simulation of experimental results for the solvent sublation of naphthalene at 25°C. In Run 1: $r_b = 0.01$ cm, $c_{1/2} = 2 \times 10^{-5}$ mol/mL, c(initial) $= 2.03 \times 10^{-7}$ mol/mL, $Q_a = 1.6$ mL/s. In Run 2: $r_b = 0.015$ cm, $c_{1/2} = 1 \times 10^{-6}$ mol/mL, c(initial) $= 2.03 \times 10^{-7}$ mol/mL, $Q_a = 1.6$ mL/s. Other parameters as in Table 3.

tool for estimating the feasibility of the removal of hydrophobic compounds of low volatility.

The ready removal of naphthalene and phenanthrene by solvent sublation suggests that this method should be suitable for the removal of other polynuclear aromatic hydrocarbons, including those resulting from coal-synfuels technology, some of which are carcinogens.

Acknowledgment

We are indebted to a grant from the National Science Foundation in support of this work.

TABLE 9
Parameters Used to Simulate Experimental Data on Naphthalene

Bubble radius (cm)	$c_{1/2}$ (mol/cm³)	V_0(expt) (ergs)	$\frac{100[V_0(\text{expt})]}{V_0(\text{calc})}$ (%)
0.01	2.00×10^{-5}	-2.51×10^{-13}	−9.0
0.015	1.00×10^{-6}	-3.71×10^{-13}	+34.4

REFERENCES

1. F. Sebba, *Ion Flotation*, Elsevier, New York, 1962.
2. B. L. Karger, in R. Lemlich (ed.), *Adsorptive Bubble Separation Techniques*, Academic, New York, 1972, Chap. 8.
3. A. N. Clarke and D. J. Wilson, *Foam Flotation: Theory and Applications*, Dekker, New York, 1983, Chap. 6.
4. T. Lionel, D. J. Wilson, and D. E. Pearson, *Sep. Sci. Technol., 16*, 907 (1981).
5. J. L. Womack, J. C. Lichter, and D. J. Wilson, *Sep. Sci. Technol., 17*, 897 (1982).
6. D. J. Wilson and K. T. Valsaraj, *Ibid., 17*, 1387 (1982).
7. K. T. Valsaraj and D. J. Wilson, *Colloids Surfaces*, To Be Published.
8. A. Seidell (ed.), *Solubilities of Organic Compounds*, Vol. 2, 3rd ed., Van Nostrand, New York, 1941, p. 647.
9. A. Seidell and W. F. Linke (eds.), *Solubilities of Inorganic and Organic Compounds*, Van Nostrand Co., New York, 1952, p. 757.
10. R. H. Perry and C. H. Chilton (eds.), *Chemical Engineer's Handbook*, 5th ed., McGraw-Hill, New York, 1973, p. 3–57.
11. A. Ralston and H. S. Wilf, *Mathematical Methods for Digital Computers*, Vol. 1, Wiley, New York, 1965, p. 98.
12. 42nd ed., R. C. Weast (ed.), *CRC Handbook of Chemistry and Physics*, CRC Press, Cleveland, Ohio, 1960, pp. 1104–1105.
13. A. Seidell and W. F. Linke (eds.), *Solubilities of Inorganic and Organic Compounds*, Van Nostrand, New York, 1952, pp. 756–757.
14. J. J. Jasper, *J. Phys. Chem. Ref. Data, 1*, 924 (1972).
15. R. H. Perry and C. H. Chilton (eds.), *Chemical Engineer's Handbook*, 5th ed., McGraw-Hill, New York, 1973, p. 3–57.
16. L. A. Girifalco and R. J. Good, *J. Chem. Phys., 61*, 904 (1957).

Received by editor April 22, 1983